Species measurements in the beam of an ionic liquid ferrofluid capillary electrospray source under magnetic stress

Kurt J. Terhune* and Lyon B. King†
Michigan Technological University, Houghton, MI, 49931

Benjamin D. Prince‡
Air Force Research Laboratory, Kirtland AFB

Nirmesh Jain§ and Brian S. Hawkett**
The University of Sydney, NSW 2006, Australia

Three solutions of an ionic liquid ferrofluid (ILFF) using 1-ethyl-3-methylimidazolium bis(trifluoromethylsulfonyl)imide (EMIM-NTf2) as the carrier liquid were emitted from a capillary electrospray source and the resulting beam was measured using a time-of-flight mass spectrometer (TOF-MS). The solutions had 3.04, 5.98, and 8.80 wt% iron oxide nanoparticles making them susceptible to magnetic fields. A Helmholtz coil was used to impose a gradient-free magnetic stress onto the electrospray source. Mass spectra were collected in the spray from each of the solutions, with and without the imposed magnetic field. The magnetic stress caused an increase in the peak intensity of distinct ion species (n = 0 or n = 1) at lower energy defects suggesting that the stress causes ions to be born at higher energy. The ratio of the ion peak intensity with magnetic field to ion peak intensity at zero magnetic field was proportional to the concentration of nanoparticles. The magnetic stress did not significantly affect the large mass distributions until the nanoparticle concentration reached 8.80 wt% in the fluid.

Nomenclature

e	=	Elementary charge
E_i	=	Particle kinetic energy
H	=	Particle mass
L_{TOF}	=	Length of time-of-flight tube
m	=	Particle mass
m/q	=	Particle mass-to-charge ratio
μ_0	=	Particle mass
M	=	Particle mass
q	=	Particle charge
q_R	=	Rayleigh limit
ρ	=	Density
r_D	=	Droplet radius
t	=	Time
t_{flight}	=	Time-of-flight
u	=	Particle velocity
V	=	Extraction voltage

*Graduate Research Assistant, Mechanical Engineering-Engineering Mechanics, 815 RL Smith Building, 1400 Townsend Drive. AIAA Student Member
†Professor, Mechanical Engineering-Engineering Mechanics, 1014 RL Smith Building, 1400 Townsend Drive. AIAA Member
‡Research Chemist, Space Vehicles Directorate, 3550 Aberdeen Ave SE, Building 570. AIAA Member
§ Research Associate, School of Chemistry and Key Centre for Polymers and Colloids, Chemistry F11
**Associate Professor, School of Chemistry and Key Centre for Polymers and Colloids, Chemistry F11

I. Introduction

WHEN monodomain ferromagnetic nanoparticles are suspended in a carrier liquid the result is a colloid which is susceptible to electromagnetic fields. The particles are typically coated with a surfactant to prohibit clumping, and are of such small size (on the order of 10 nm) that Brownian motion prohibits sedimentation caused by external body forces.[1] Subjecting a ferrofluid to a strong magnetic field causes the magnetic moments within the colloid to attempt to align with the magnetic field lines Perturbations along a free surface of the colloid cause local concentrations of the magnetic field. The concentration of the magnetic field attracts the nanoparticles and an instability forms that causes the liquid to bulge at the locations of concentrated magnetic field known as a Rosensweig instability[1,2]. The instability is balanced by the surface tension of the fluid which pulls against this change in the liquid surface. The end result is an arrangement of static fluid peaks on the surface of the ferrofluid, seen in Figure 1. A particularly interesting class of ferrofluids have recently been synthesized from ionic liquid (IL) carrier fluids.

ILs are room-temperature molten salts with high electrical conductivity and almost zero vapor pressure, making them ideal for operating in a vacuum., Because they are comprised of both anions and cations they can be manipulated by electric fields.[3] Due to these attributes ILs have become a candidate propellant for satellite propulsion.[4-9] Ferrofluid electrospray propulsion from a Rosensweig instability pattern was first demonstrated by Meyer and King in 2013[10,11] using an ionic liquid ferrofluid (ILFF) developed by Jain *et al.*[12] Such a device is intriguing because the spray emitter tips are essentially "made of" their own propellant with no underlying solid needle. Further electrospray emission studies used an ILFF also developed by Jain et al., which substituted the ionic liquid Ethylammonium Nitrate (EAN) with 1-Ethyl-3-methylimidazolium bis(trifluoromethylsulfonyl)imide (EMIM-NTf2).[11] The substitution was done to reduce the viscosity of the ILFF and reduce the formation time of the Rosensweig instability peaks.

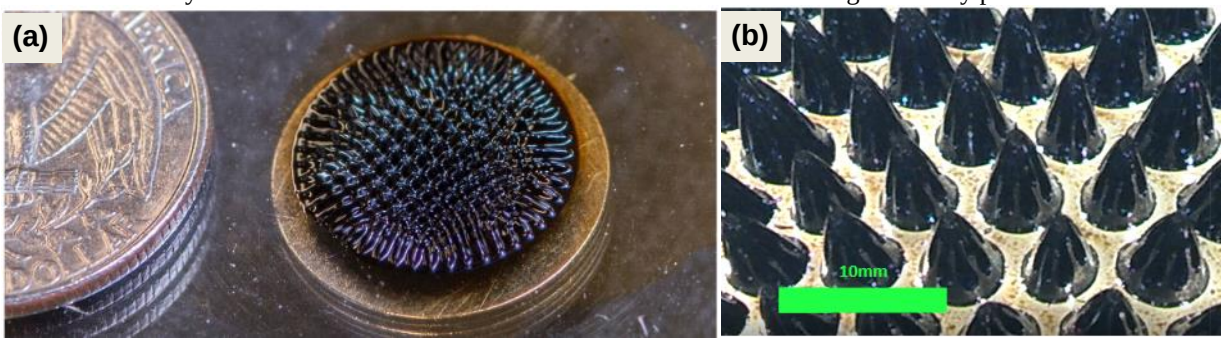

Figure 1. Images of the Rosensweig instability in a FerroTec EFH-1 ferrofluid.[10]

Terhune *et al.*[13] reported on species measurements of particles emitted from an ILFF electrospray source in 2014. Witness plates from these experiments indicated that the beam consisted of more than pure ionic liquid ions and droplets, and is more likely some combination of ions, nanoparticles, and pure ionic liquid droplets. However, direct evidence of droplets was not present in the mass spectrometer data due, possibly, to instrument limitations

Though the results of these experiment showed that ILFFs could be emitted from the static Rosensweig peaks, removing the need for a backbone structure (hollow capillary or solid needle), Terhune's early experiments did not provide a systematic set of data comparing ILFF spray to that of "neat" ILs, meaning ILs having no nanoparticles in suspension, and thus various effects were convolved in the measured data.

II. Goal of Study

The mass spectra of neat IL electrosprays have been collected and studied extensively.[14-17] Similar measurements have not been reported for capillary electrospray sources running ILFFs, nor have they been done while applying an external magnetic field to the source. Such measurements would provide a means to directly compare ILFF electrospray to the traditional neat IL electrospray.

Research reported here had two goals: (1) determine how the presence of magnetic nanoparticles suspended in an IL affects the resulting electrospray emission when compared with neat IL; (2) determine how an applied magnetic field changes the composition of an ILFF electrospray beam compared to magnetic-field-free spray.

III. Background

A. Ferrofluids

The magnetic nanoparticles that form a ferrofluid maintain their stable colloidal nature due to their small size and the polymer surfactant which coats them. The selection of the surfactant is dependent on the material and surface structure of the nanoparticles, along with the surfactant's affinity with the carrier liquid. As such many materials have been used to provide particle stabilization,[12,18,19] but a standard surfactant has both a polar absorbent which anchors to the nanoparticle and a non-polar tail which is soluble in the carrier liquid. The dispersant chosen to stabilize the magnetic particles in the ionic liquid EMIM-NTf2 is a block copolymer 10MAEP-60DMAM, which is comprised of 10 poly(monoacryloxyethyl phosphate) (PMP) blocks, a RAFT end group ($CS_3C_4H_9$), 60 poly(N,N-dimethylacrylamide) (PDA) blocks, and a functionalizing group ($CH_3CHCOOH$). The former two parts of the molecule make up the absorbent anchor, and the latter two are the soluble stabilizers which provide steric stabilization. The process to synthesize the ILFF is described by Jain et al.[18] and King et al.[20]

B. Ionic Liquid Ferrofluid Electrosprays

Two forms of ILFF electrosprays have been studied – electrospray from a "needle-free" ILFF peak formed by the Rosensweig instability, and electrospray from a capillary needle with and without an applied magnetic field.[21] Electrosprays from the Rosensweig instability have been produced from a single peak,[13,20,22] and arrays of five,[10,11,20] seven,[23] and eight[23] peaks. In each of these electrospray studies, visual inspection of the residue from electrospray emission onto the extraction electrode revealed evidence of the magnetic nanoparticles. The introduction of these nanoparticles in the ILFF inherently changes its fluid properties and consequently the emission of an ILFF spray differs from that of a neat ionic liquid even without application of a magnetic field.[24] Madden et al.[21] also observed that the addition of a magnetic field extends the stability range to lower flowrates, currents, and voltages for ILFF electrosprays. Lower flowrates result in a smaller Taylor jet diameter, and consequently the production of smaller droplets.[25]

C. Mass Spectrometry of Electrospray Propulsion Systems

Mass spectrometry is a standard method of analyzing the emission of electrospray thrusters to predict their performance in space propulsion applications.[14,17,26-29] A mass spectrometer can measure the value of m/q for species emitted from these thrusters. A quantitative understanding of the m/q of an electrospray thruster is paramount in designing a thruster for specific missions. It can determine whether the thruster can be used in a high thrust-to-power mission or a high Isp mission, or instead provides variable m/q to satisfy both types of missions.

An orthogonal extraction TOF mass spectrometer pulses an extraction/acceleration electrode (V_i) placed perpendicular to the axis of the electrospray beam to capture a volume of the beam and accelerate it, with a narrow kinetic energy range, toward a charge-exchange multiplier (CEM). The difference in time of the initial pulse and the time of the signals gathered by the CEM are used to determine the flight time of the various particles in the volume of the electrospray beam, under the assumption that all particles have approximately the same kinetic energy once extracted. The time-of-flight of the particles can be directly related to their mass-to-charge ratios (m/q) through the relationship between the electrical and kinetic energy of the particles, Eq. 1.

$$\frac{1}{2}mu^2 = qeV \tag{1}$$

Rearranging Equation 1 for mass-to-charge results in $\frac{m}{q} = \frac{2V}{u^2}$. Substituting the length of the TOF chamber (L_{TOF}) divided by the time-of-flight (t_{flight}) for the velocity and solving for m/q, one derives a relationship for the mass-to-charge ratio of the particles based on their flight time through the TOF chamber, Eq. 2.

$$\frac{m}{q} = \frac{L_{TOF}^2}{t_{flight}^2 2V} \tag{2}$$

IV. Experimental Facilities and Methods

Experiments using a capillary electrospray apparatus were conducted in the time-of-flight mass spectrometer facility (TOF-MS) at the Air Force Research Laboratory (AFRL) on Kirtland Air Force Base. The specifics of the

testing facility, the electrospray apparatus, electrospray fluids, and the Helmholtz coil are described, respectively, in sections IV-A, IV-B, IV-C, and IV-D. The procedures for the experiments are described in section IV-E.

A. Time-of-flight Mass Spectrometer Facility

The AFRL houses an orthogonal reflectron TOF-MS that can detect particles in the range of a few amu/e to over 1,000,000 amu/e. The facility is a 1-meter long by 0.254-meter wide by 0.254-meter tall reflectron flight-tube detection chamber that is situated orthogonal to a 0.5-meter long source chamber. A multichannel plate (MCP) is used as the detector and is positioned at both ends of the reflectron flight-tube to provide both linear and reflectron TOF measurements. The apparatus has been described in detail by Miller *et al.*[30] *T*he source chamber is maintained at a pressure of 10^{-7} Torr, while the detection chamber is maintained at approximately 2 x 10^{-8} Torr. The pressures are achieved using two 250 l/s turbo-molecular pumps backed by one 600 l/min dry scroll pump.

The TOF-MS also contains multiple lenses, grids and deflectors, attached at the end of the source (discussed in section IV-E) which are used to maximize the beam intensity entering the TOF pulsing region. The pulsing region consists of a pair of parallel plates which are parallel to, but offset from, the beam axis. Each plate has a gridded aperture to allow orthogonal transmission of ion species when the voltages on the plates are pulsed. Continuing along the original beam axis, a quartz crystal microbalance (QCM), used to quantify the mass flow rate, and a Faraday cup, used to measure the current of the beam, are located after a 6 mm rectangular aperture at the end of the parallel plates. These devices are positioned by means of a linear translation stage allowing rapid switching of the two devices. The QCM provides a measure of the mass flow rate of electrospray by measuring the accumulation of a uniform layer of the condensed beam products on a quartz crystal. The additional layer changes the natural frequency of the crystal which is directly translating to thickness-, or mass accumulation-, per-second. The maximum detectable mass flow rate on the QCM is on the order of 100 ng/s.

B. Capillary Electrospray Source

The capillary electrospray source, shown in Figure 2 a., produced the electrospray beams analyzed in the TOF-MS facility. The source is comprised of (1) and extractor plate which has a 1-mm-diameter aperture, (2) a 50-cm long, 75-µm-inner diameter capillary needle, with a wall thickness of ~5 µm at the needle apex, (3) a PTFE block to both hold and isolate the needle, and (4) set screws to align the needle with the extractor aperture. The IL or ILFF was fed to the capillary needle by pressurizing a vial of liquid outside the vacuum facility. A set pressure, p_0, was accomplished by opening or closing valves which either fed nitrogen gas into the vial or removed gas from the vial via a mechanical scroll pump. The liquid was biased via an electrode inserted into the vial. The feed system is shown in Figure 2 b. The flowrate of the liquid being fed to the capillary source was determined via the bubble method, wherein the velocity of a bubble introduced in the feedline was measured for a given vial pressure. The velocity was then converted to volumetric flowrate using the known dimensions of the capillary tube.

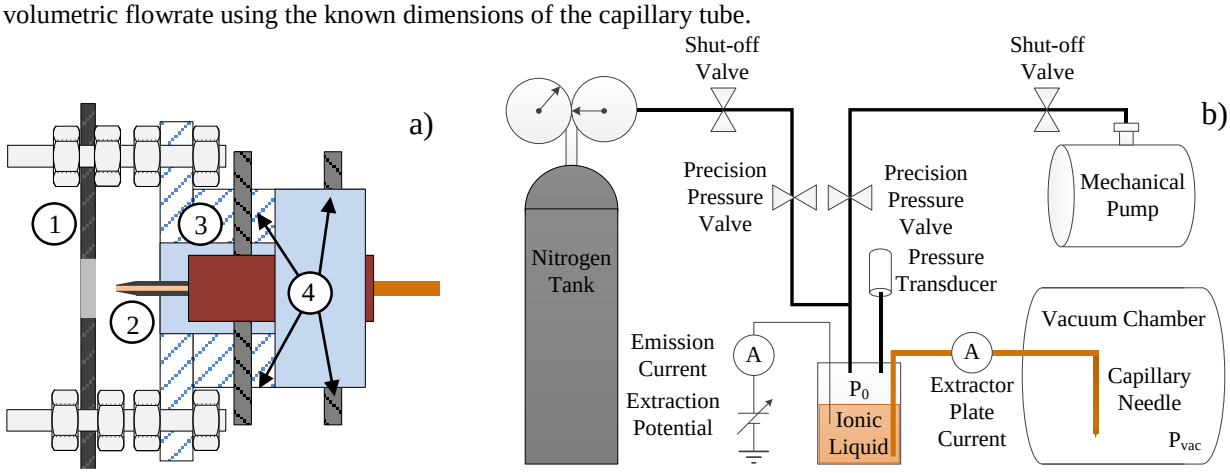

Figure 2. (a) Capillary electrospray source comprised of (1) extractor plate, (2) capillary needle, (3) PTFE isolation block, (4) alignment set screws. (b) Schematic of the capillary source pressure feed system.

C. Electrospray Fluids

Four fluids were used throughout the various experiments reported in Section V. They are the neat IL EMIM-NTf2, and three solutions of EMIM-NTf2 ferrofluid with varying concentration of magnetic nanoparticles. The ferrofluids will henceforth be called ILFF-10, ILFF-20, and ILFF-30 based on the volume percent of a concentrated

parent ILFF that was mixed with neat IL. The parent ILFF contained 26.0 wt% iron oxide nanoparticles which led to nanoparticle concentrations in the five solutions of 3.04, 5.98, 8.80 wt% for ILFF-10, ILFF-20, and ILFF-30, respectively. The volumes of neat IL and ILFF, and nanoparticle concentrations that comprised each solution are tabulated in Table 1.

Table 1. Diluted ILFF Solutions used in the TOF-MS experiments.

ILFF Dilution	Volume neat IL (mL)	Volume ILFF (mL)	Total Volume (mL)	Nanoparticle Concentration (% wt/wt)
Neat IL	NA	NA	NA	0.00
ILFF-10	0.18	0.02	0.2	3.04
ILFF-20	0.16	0.04	0.2	5.98
ILFF-30	0.14	0.06	0.2	8.80
Parent ILFF	NA	NA	NA	26.00

D. Magnetic Field

A Helmholtz coil provided a variable magnetic field that could be applied to the source for several minutes at a time. The solenoid design was chosen to provide a gradient free field thus removing the effect of a Kelvin force, Equation 3, at the emission site.

$$\text{Kelvin force density} = \mu_0 M \nabla H \tag{3}$$

The Helmholtz coil consists of two 19-cm-diameter, 500-wrap coils separated by a distance of 10 cm. The coils required cooling to prevent the radiative heat from affecting the operation of the electrospray source; two methods were used: a water-cooled jacket lining the center wall of the coils, and forced air convection using a box fan. The Helmholtz coil assembly was concentrically aligned over the exterior of the source vacuum envelope using set screws. Figure 3 shows the Helmholtz coil assembly attached to the source flange of the TOF chamber.

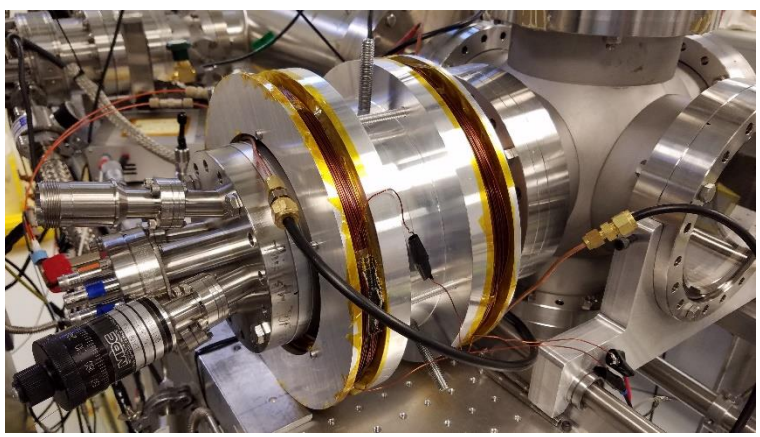

Figure 3. Helmholtz coil assembly attached to the source flange of the TOF-MS facility. The Helmholtz coil was capable of producing 200 Gauss at 5 Amps.

E. Experimental Methods

The following procedure was use to complete the experiment using the TOF-MS. The time-of-flight instrument is described in full detail elsewhere[30] so it will only be briefly described here. The emission axis (axial) was described above in IV-C and consists of lenses, deflectors, the parallel extraction plates, and the translation stage containing the Faraday cup and QCM. The transverse axis begins beyond the parallel extraction plates with an Einzel lens located 6 mm from the time-of-flight extractor pulsing plate, with the front and back lens potential of the Einzel fixed at ground. Beyond the Einzel lens is a simple horizontal deflector that allows the ion beam into the main field-free flight tube. At the end of the tube, a series of grids turn the ion beam around and direct it to the MCP used to generate event pulses

which are sent through two channels of a pre-amplifier and onto a multi-scalar card for generation of the time-of-flight mass spectrum.

The parallel pulsing plates constitute the extraction region. The parallel pulsing plates are first given a base DC offset that serves to retard the ions in the middle of the extraction zone. When a pulse is active, one plate (the repeller) is given a greater potential than the other, which serves to repel the ions toward the time-of-flight extractor plate. Successful passage through the aperture in the extractor plate yields additional acceleration as the front component of the Einzel lens is held at ground. For example, consider the emission source being biased at +900 V, and the base DC potential at +880 V. Ions in the middle of the extraction region will have approximately 20 eV axial kinetic energy at the center of the extraction region, assuming they are emitted at the nominal bias potential. If these ions are in the center of the extraction region during an active pulse event of +400 V, the repeller will have a +1280 V potential, while the time-of-flight extractor plate will maintain +880 V. If an ion successfully passes the extractor plate, it will net approximately 1080 eV of transverse kinetic energy by the end of the Einzel lens.

The DC offset potential on the pulse plates transforms the instrument into an energy sensitive analyzer. Simulations have shown that ions with residual axial kinetic energies of greater than 20 eV, regardless of m/q, cannot traverse the flight tube without collision with the instrument walls. The wide range of axial kinetic energies at which ion and droplet species are emitted means that only those particles within a small energy difference from the pulsing plates are slowed properly for entrance into the flight tube, (see Miller et al.,[30] for further discussion on this topic). To ensure the measurement of a majority of the emitted particles, spectra needed to be collected for varying pulsing-plate potentials corresponding to varying particle energies. This was achieved by decreasing the pulsing plate bias in 50-V increments from a maximum of 850 V (equal to the maximum possible particle energy set by the reservoir bias) to the bias that had a Faraday current of 50 percent of the maximum magnitude (the Faraday cup current magnitude when the pulsing plates were at ground) and/or provided a mass spectrum that had measurable droplet distributions. General operation of the instrument is described thusly: once stable electrospray emission was established the optics were optimized to provide maximum current signal on the Faraday cup. The parallel plates were then pulsed and ions were introduced into the TOF flight tube and subsequently counted. The pulse width and magnitude were 100 μs and 400V, respectively. The pulse width greatly affects the size of particles gated into the chamber, as heavy particles must fully escape the extraction region before the end of the pulse in order to be counted. As a result, the pulse length used for these experiments was 100 μs to allow particles up to 1,000,000 amu/e; an expected maximum range for ILFF droplet distributions.

For every pulsing plate potential one mass spectrum was collected while the electrospray source operated without an applied magnetic field. This was followed immediately by a spectrum while a 200-Gauss magnetic field was applied to the source. A final spectrum was collected after the removal of the magnetic field as a means to verify reproducibility of the mass spectra taken at the same operating conditions. The Helmholtz coil could only be operated continuously for approximately 5 minutes before heating became a factor. It required roughly 10 minutes to cool prior to another extended period of operation. This was the limiting factor in the time required to collect a single mass spectra scan. A single mass spectrum consisted of 50,000 pulse cycles collected at a rate of 200 Hz. This work is not focused on identifying those ions emitted at various energy defects, defined here as axial kinetic energies below the electrospray bias potential. As such, the spectra taken at each energy defect for a given flow rate have been directly summed to approximate the entire mass spectrum of the emitter. The presented figures are the result of this summation and are termed the "integrated time-of-flight spectrum".

Mass spectra scans were collected following the procedure described above for three flowrates, approximately 0.5, 0.75, and 1.0 nl/s, using ILFF 10, ILFF 20, and ILFF 30 solutions.

V. Results

Mass Spectra of Ionic Liquid Ferrofluid Electrospray Sources

Results of the TOF-MS experiments consist of mass spectra of the beam emitted from a capillary electrospray source running on the three ILFF solutions: ILFF-10, ILFF-20, and ILFF-30. Also reported below are the mass spectra collected while the electrospray source was subjected to a 200-Gauss, externally-applied magnetic field.

Table 2. Vial pressures and flowrates used in the mass spectrometer experiments for the neat IL and ILFF solutions. The flowrates were derived via the bubble method.

ILFF Solution	Vial Pressure (Torr)	Flowrate (nl/s)
Neat IL	100	0.63
	150	0.95
	200	1.26
ILFF-10	100	0.52
	150	0.78
	200	1.04
ILFF-20	100	0.47
	150	0.71
	200	0.94
ILFF-30	150	0.54
	200	0.72
	250	0.9

Integrated time-of-flight mass spectrum of the electrospray beam emitted from the capillary source using the ILFF-10, ILFF-20, and ILFF-30 solutions were collected for each of the flowrates reported in Table 2. The pulsing plate base potentials ranged from 500 V to 850 V for flowrates 0.47 nl/s, 0.52 nl/s, 0.54 nl/s, 0.71 nl/s, 0.72 nl/s and 0.90 nl/s; and 450 V to 850 V for flowrates 0.78 nl/s for 0.94 nl/s. and 1.04 nl/s. The integrated time-of-flight spectrum, as described in the penultimate paragraph of IV-E, for each of the three flowrates were normalized such that the n = 0 peak equaled an arbitrary intensity of 1e5, and are shown in Figure 4 a) for ILFF-10, Figure 5 a) for ILFF-20 and Figure 6 a) for ILFF-30. The three lighter mass peaks in the spectrum are the cation species, $EMIM^+$, [EMIM-NTf2] $EMIM^+$, and $[EMIM\text{-}NTf2]_2$ $EMIM^+$, denoted, respectively, as n = 0, n = 1, and n = 2 in Figures 4, 5, 6, and 8. Cation species of $[EMIM\text{-}NTf2]_3$ $EMIM^+_2$, $[EMIM\text{-}NTf2]_4$ $EMIM^+_3$, $[EMIM\text{-}NTf2]_5$ $EMIM^+_4$, $[EMIM\text{-}NTf2]_6$ $EMIM^+_5$, and $[EMIM\text{-}NTf2]_7$ $EMIM^+_6$ (n = 3, 4, 5, and 6, respectively) were also observed in the ILFF-10, ILFF-20, and ILFF-30 mass spectra. Large mass distributions are centered at approximately 40,000 amu/e and 150,000 amu/e for ILFF-10, 6,000 amu/e, 40,000 amu/e and 150,000 amu/e for ILFF-20; the distributions at 40,000 amu/e and 150,000 amu/e are indiscernible in the ILFF-30 spectra.

Integrated time-of-flight mass spectra of the electrospray beam emitted from the capillary source using the ILFF-10, ILFF-20, and ILFF-30 solutions were also collected with the magnetic field applied. The integrated time-of-flight spectrum for each of the three flowrates were normalized such that the n = 0 peak equaled an arbitrary intensity of 1e5, and are shown in Figure 4 a) for ILFF-10, Figure 5 a) for ILFF-20, and Figure 6 a) for ILFF-30.

In figures 4, 5, and 6, the main plot displays the low-mass range (0 to 1500 amu/e) with the spectra for the middle and upper flowrates shifted on the m/q axis by 20 and 40 amu/e, respectively, for ease of comparison, while the inset plot displays the high mass range of the un-shifted spectra, (1,000 to 1,000,000 amu/e).

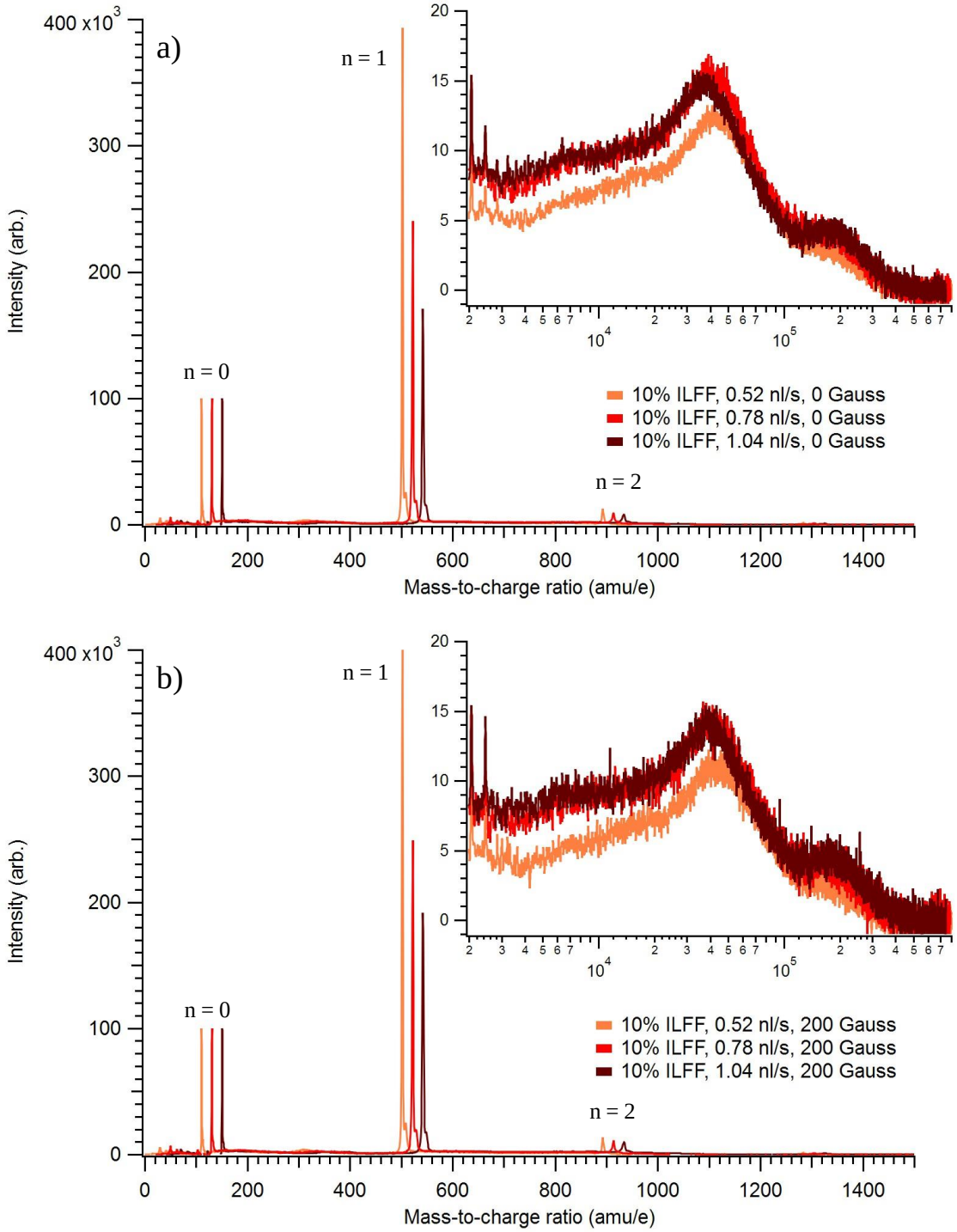

Figure 4. Mass spectra of an electrospray emitted from the capillary source using ILFF-10 under zero applied magnetic field (a), and under a 200 Gauss magnetic field (b). The spectra in the low-mass plot (0-1500 amu/e) have been incrementally shifted by 20 amu/e to ease comparison.

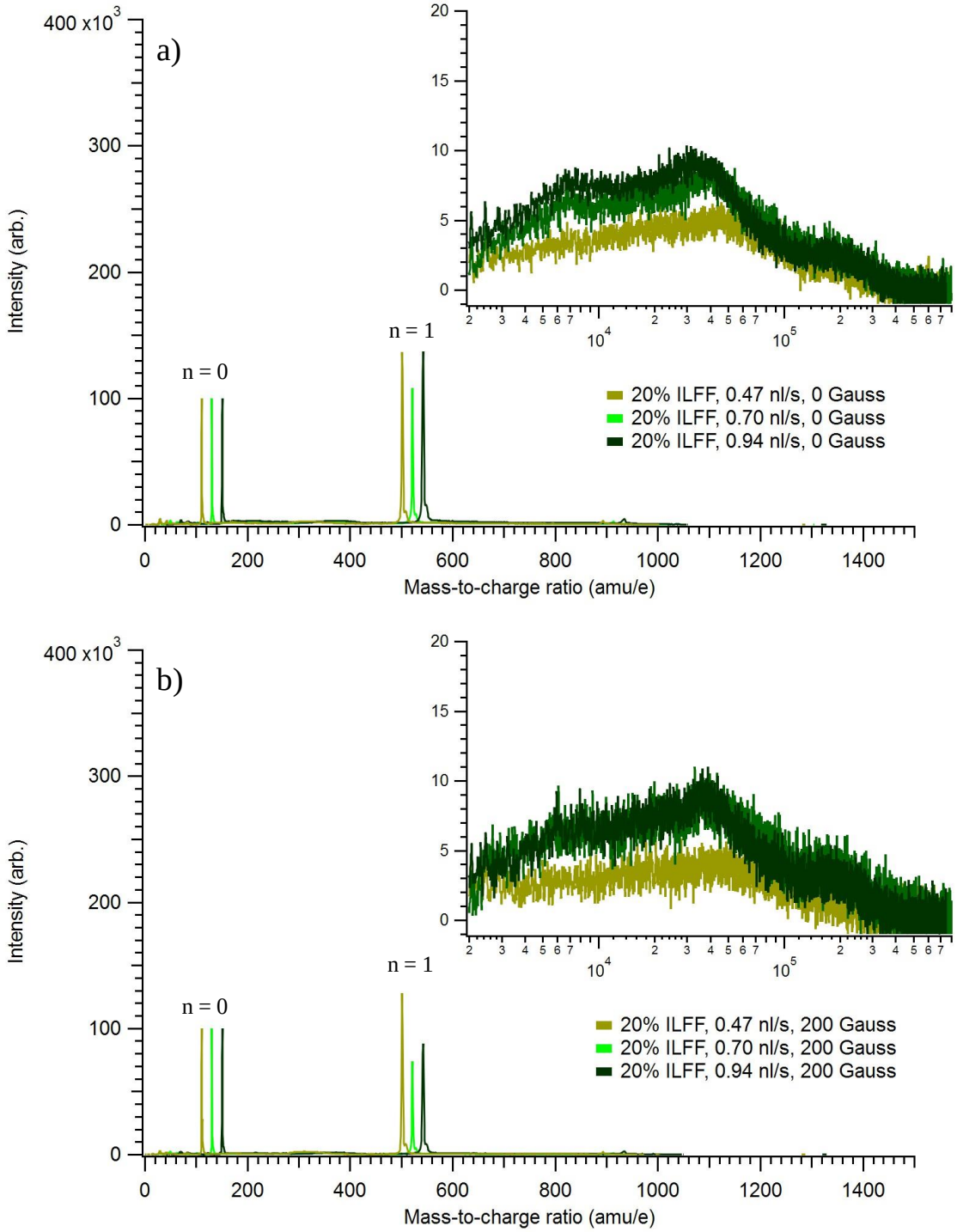

Figure 5. Mass spectra of an electrospray emitted from the capillary source using ILFF-20 under zero applied magnetic field (a), and under a 200 Gauss magnetic field (b). The spectra in the low-mass plot (0-1500 amu/e) have been incrementally shifted by 20 amu/e to ease comparison.

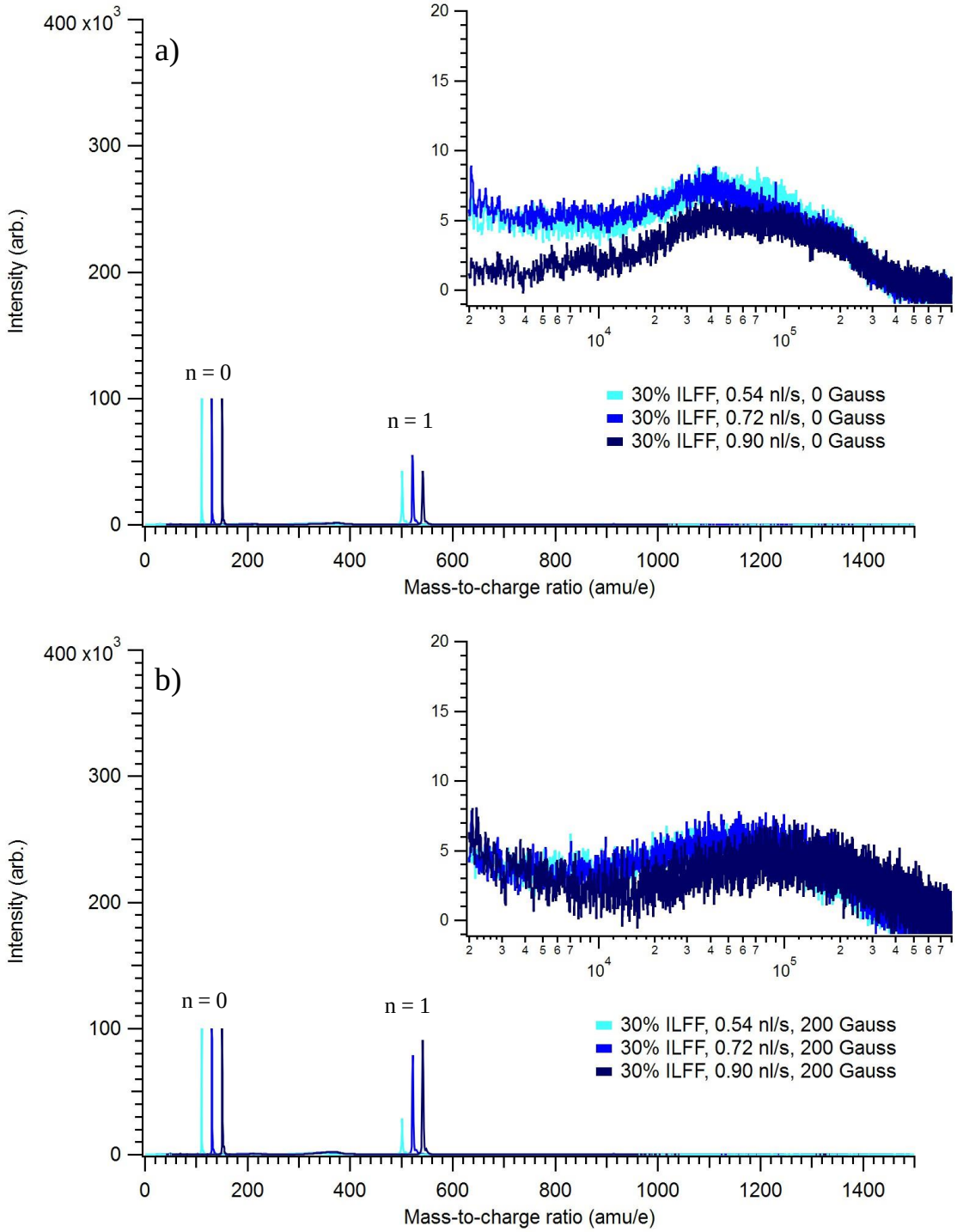

Figure 6. Mass spectra of an electrospray emitted from the capillary source using ILFF-30 under zero applied magnetic field (a), and under a 200 Gauss magnetic field (b). The spectra in the low-mass plot (0-1500 amu/e) have been incrementally shifted by 20 amu/e to ease comparison.

VI. Discussion

The results in section V document the mass spectra of several solutions of ILFF electrosprayed from a capillary source under various operating conditions. Several observations on the spectra will be discussed in further detail as they pertain to the changes made throughout in the operating fluid and operating conditions of the electrospray source.

A. Intensity Axis and Spectra Repeatability

The intensity axis of the mass spectra can provide a reasonable method to compare multiple scans and realize changes within the beam of the electrospray. However, there is uncertainty on the repeatability of the peak intensities between individual scans. To determine the repeatability at least two mass spectra, consisting of 50,000 scans, were collected for each energy defect while operating the electrospray without the applied magnetic field. The magnitude of the peak intensities, along with the intensity ratios of the n = 1 to n = 0 peak, was measured for each mass spectrum. The variability of both the peak intensity and the peak intensity ratio between the two (or more) spectra collected at energy defect were calculated as one standard deviation from the average. Figures 7 a) and b) give the standard deviation as a percentage of peak intensity and peak intensity ratio, respectively, for each ion energy at the lowest flowrate of each solution. The standard deviation in peak intensity and peak intensity ratio provide the measure of repeatability in collecting mass spectra. Therefore, any conclusions based on the comparisons of different spectra must take into account this variability, which is illustrated as ±error (30-percent for peak intensity and 20-percent for peak intensity ratio) in the curves of Figure 8 b), 9, 10, and 11.

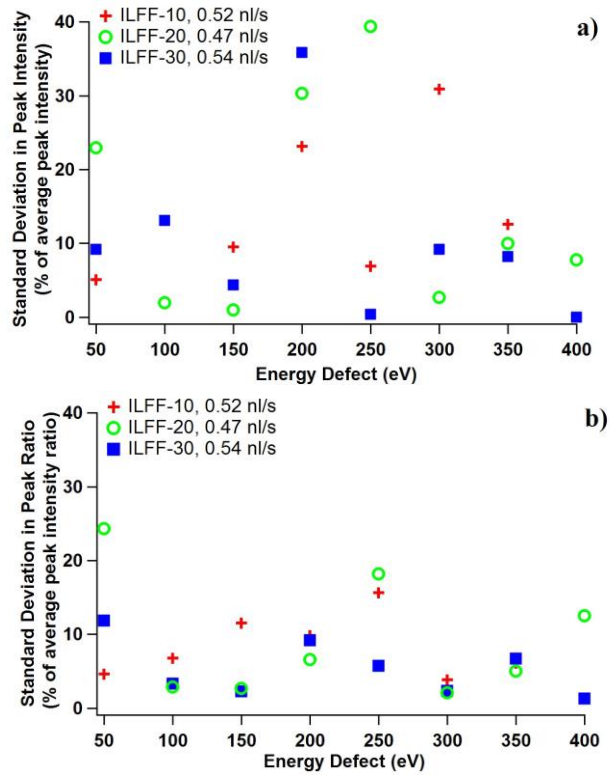

Figure 7. Standard deviation as a percentage of (a) average peak intensity, (b) average peak intensity ratio of mass spectra collected under the same conditions.

B. Effect of Nanoparticle Concentration on Mass Spectra

Comparison of the mass spectra collected for each ILFF solution shows a correlation between the relative intensities of masses present in the emitted electrospray beam and the concentration of magnetic nanoparticles in the source fluid. Specifically, as the concentration increases the ratio of n=1 to n=0 ion species decreased significantly, illustrated by the change in ion peak intensities in the ILFF-10, ILFF-20 and ILFF-30 electrospray mass spectra in Figure 8 a). While running on ILFF-10, the electrospray had a significant amount of the n = 0, n=1, and n = 2 ion species, with the n = 1 species being the most prominent. When the ILFF-20 and ILFF-30 solutions were used there was no longer a significant amount of n = 2 ion species in the beam, with the n = 0 and n = 1 ion species approximately equal in intensity for the ILFF-20 solution, and the n = 0 peak the most prominent for the ILFF-30 solution. This suggests that the mass of the species emitted from the beam decreases with the increase in nanoparticle concentration. Further evidence of this trend was observed in the large masses, illustrated in Figure 8 b). Curve fits are also shown to better clarify multiple distributions in the high-mass range of the mass spectra. They are in the form of Log normal fits which represent the Boltzmann distributions of a droplet species. While two large mass distributions exist at approximately 40,000 amu/e and 150,000 amu/e for an electrospray running on all three ILFF solutions, the relative intensity decreases by nearly 50-percent for the two solutions with higher ILFF concentrations. In Terhune et al.[24] it was reported that electrosprays running the same ILFF solutions observed an increase in emission current with the increase nanoparticle wt%. Given the reported increase in emission current, and the combination of a shift to lighter ion species in a) and the reduction of the droplet peaks in b) suggest that the composition of the beam shifts from larger to smaller m/q with the increase in nanoparticle concentration.

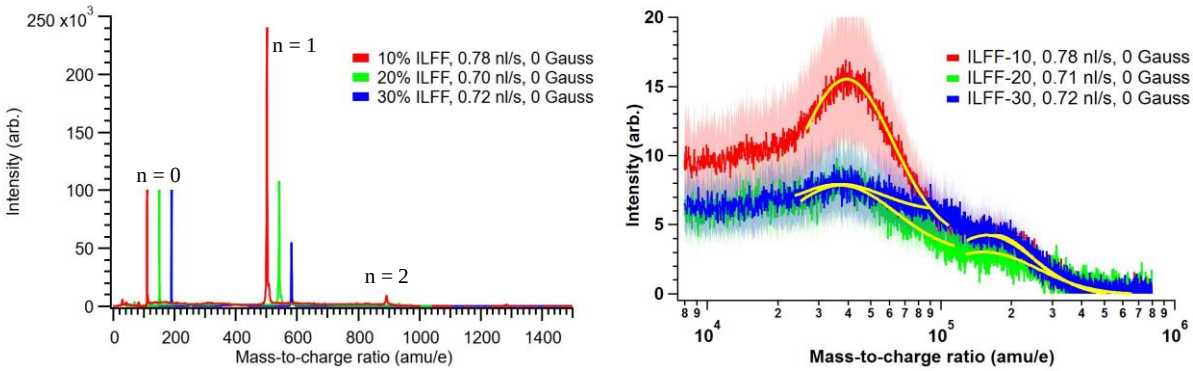

(a) **(b)**

Figure 8. a) Comparison of mass spectra from electrosprays running on ILFF-10, ILFF-20, and ILFF-30 solutions normalized to n = 0 peak. The spectra from ILFF-20 and ILFF-30 solutions have been shifted on the mass axis by 40 and 80 amu/e, respectively for ease in comparison. b) Mass spectra of ILFF-10, ILFF-20, and ILFF-30 solutions with log-normal curve fits (yellow) to distinguish the droplet distributions.

The nanoparticle size could affect the emitted droplet size of the electrospray. In neat IL electrosprays, the droplet size is theoretically determined through the Rayleigh limit, $q_R = 8\pi\sqrt{\varepsilon_0 \gamma r_D^{\,3}}$, of a liquid drop, i.e. the amount of charge a droplet can maintain before the electric stress the charge produces overcomes the surface tension of the liquid. The limit is dependent on the surface tension and the radius of the liquid drop. In IL electrosprays, the mean charge of the droplets from electrosprays is known to be approximately 40-percent of the Rayleigh limit.[4,31,32] The mass of a droplet can also be expressed in terms of the droplet radius, $m = 4/3\rho\pi r^3$. Therefore, if the mass-to-charge ratio, density, and surface tension of a liquid drop is known, the radius of the droplet can be derived. The two droplet distributions observed in this research were approximately 40,000 and 150,000 amu/e, and the surface tension and density of EMIM-NTf2 at 300K are 0.0356 N/m and 1523 kg/m^3, respectively. This gives droplet radii of 5 nm and 12 nm, respectively, for the 40,000 and 150,000 amu/e distributions, indicating that the droplet size of the neat IL electrospray is on the same order as the nanoparticles added to create the ILFF. Consequently, the finite size of the nanoparticles must certainly affect the jet-droplet breakup instability, changing the m/q of the emitted electrospray beam.

C. Effect of Magnetic field on Mass Spectra

Comparison of the ILFF electrospray with and without the application of a magnetic field reveals that the magnetic field has little statistical effect on emitted mass species. The change in relative intensity of the 40,000 amu/e distribution in the ILFF-30 spectra was the only statistically significant effect of the application of the magnetic field, which resulted in a 40 percent decrease in the intensity when compared with the zero-field case. The mass spectra of this case is shown in Figure 9, with Log Normal fits overlaying the curves to distinguish the two mass distributions. Given that a magnetic effect of the intensity exists for the ILFF-30 solution, further investigation is warranted, albeit using a more repeatable method to collect the mass spectra, to determine if there a similar magnetic effect exists for all large mass distributions.

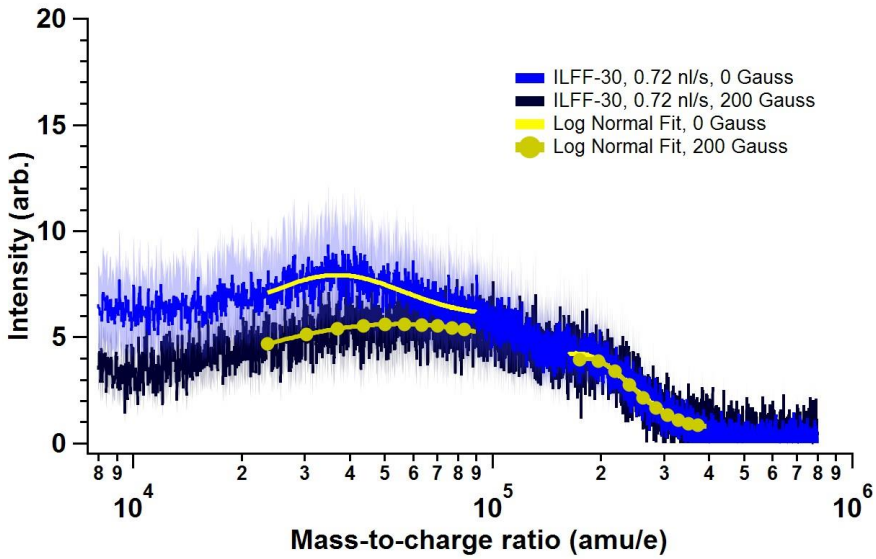

Figure 9. Log normal curve fits for droplet distributions collected from an electrospray operating at approximately 0.75 nl/s using ILFF-10, ILFF-20, and ILFF-30 solutions, with and without a 200-Gauss magnetic field.

Another metric used to quantify the effect of the magnetic field was the ion-peak-intensity ratio (Int_B/Int_{noB}), which is the ratio of the peak intensity of an ion species from a spectrum collected with magnetic field applied over the peak intensity of the same ion species from a spectrum collected when there is zero magnetic field. This ratio quantifies the shift in m/q of the electrospray; a larger Int_B/Int_{noB} indicates a shift towards lighter ion species (n = 0) when the magnetic field is applied. The Int_B/Int_{noB} was determined for the spectra collected at each VA2 potential (axial energy defect) that made up the integrated spectra, and depicted in Figure 10 a) through c).

Figure 10 illustrates how the pulsing plates can be used as a retarding potential analyzer (RPA); in doing so it shows a correlation exists between the magnetic field strength and the kinetic energy of the ions emitted from the electrospray sources. For ILFF-10, ILFF-20, and ILFF-30 the Int_B/Int_{noB} is larger for energy defects between 200 and 300 eV, greater than zero for the middle range of energy defects, and near 1 for the lowest energy defects. This trend seems to be accentuated with the increase in nanoparticles. A larger Int_B/Int_{noB} at smaller energy defects indicates that a larger percentage of the ions are born at higher energies.

An explanation for this would be the reduction in the Taylor cone-jet length. The emission site of ions and droplets in electrosprays is well-studied.[25,32-34] The current understanding places ion emission at two regions of the emission site, (1) the transition region[35,36] between the Taylor cone, formed by the balance of surface tension and electric stress, and the Taylor jet, the resultant ejection of mass that forms after the electric stress exceeds the surface tension of the emitted liquid, and (2) the terminus of the Taylor jet.[25,37] In a study of the ion emission of a EMIM-NTf2 electrospray Gamero-Castaño found that ions were emitted from both of these regions.[25] Furthermore, he found that the voltage along the length of the Taylor jet dropped significantly (ranging from 208V to 647 V for a 1700-V extraction potential), suggesting that the jet is not equipotential with the Taylor cone. Therefore, ions born in the latter region of the cone-jet it will have less energy than those born near the transition region. As the ILFF solutions are not a pure liquid, it is possible that the jet dynamics have changed, possibly reducing the jet length, or the prominent emission location of the ions. The magnetic nanoparticles are known to be very monodisperse with a diameter of approximately 30 nm, whereas highly conductive electrosprays have jet diameters of 26 to 49 nm for the range of flowrates used in these experiments.[25]

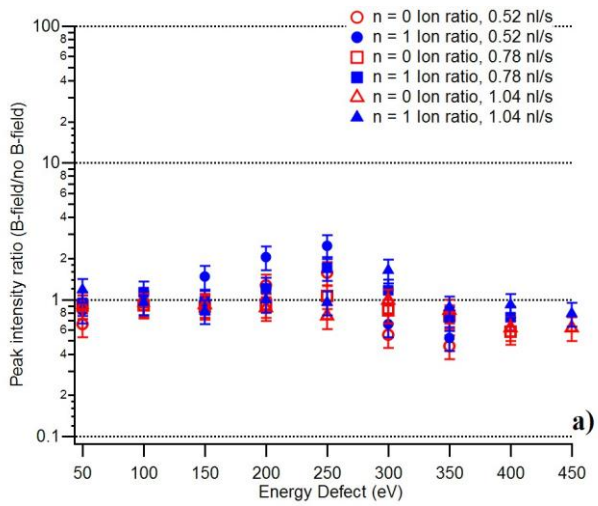

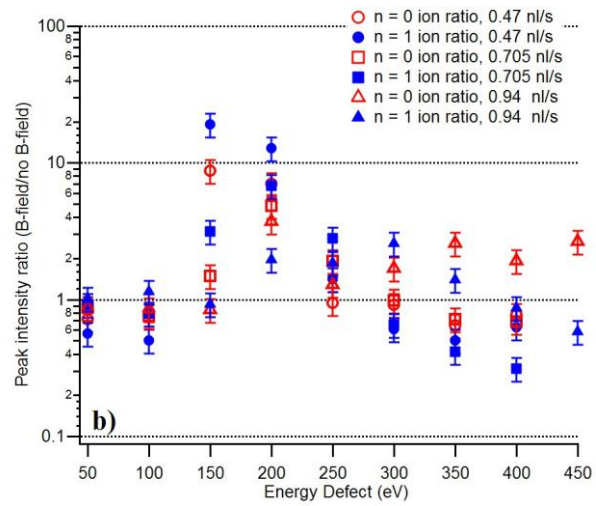

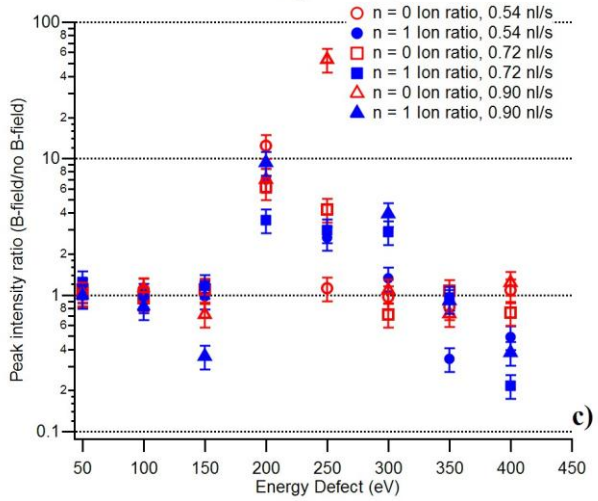

Figure 10. Ratio of ion peak intensity ratios for spectra collected plotted against the energy defect from maximum of 900 eV using (a) ILFF-10, (b) ILFF-20, and (c) ILFF-30 as the working fluid.

VII. Conclusion

A capillary electrospray source was operated using a neat IL propellant and five solutions of an ILFF propellant and the resulting beam was measured using a TOF mass spectrometer. The parent ILFF was comprised of 26.0 wt% iron oxide nanoparticles, 4.6 wt% copolymer, and 69.4 wt% EMIM-NTf2. The solutions of ILFF were produced by adding 10, 20 and 30 % (v/v) to the neat IL which resulted in nanoparticle concentrations of 3.04, 5.98, 8.80 wt%, respectively. The same capillary source, running on the same six propellants, was then subjected to a 200-Gauss magnetic field concentrically aligned with the capillary needle and the resulting beam also measured using a TOF mass spectrometer. The magnetic field was produced using a Helmholtz coil to create a gradient-free field within its the hollow core. The resulting mass spectra were shown to be dependent on two new variables, the nanoparticle concentration and the applied magnetic field.

Mass spectra of the ILFF solutions revealed that both small mass species and large mass distributions exist in an electrospray running on such fluids. The small mass species were the cation species of EMIM-NTf2, with $[\text{EMIM-NTf2}]_n\,\text{EMIM}^+$, for n = 0, 1 in all spectra, with n = 2, 3, 4, and 5 in solutions with lower nanoparticle concentration. Two or three large mass distributions were measure at approximately 6,000 amu/e, 40,000 amu/e and 150,000 amu/e. The relative intensities of both the small mass species and large mass distributions were dependent on the concentration of nanoparticles. A shift in the intensities was observed where the larger masses distribution dropped, while the small ions species increased in intensity. It is thought the nanoparticles interact with the jet breakup dynamics causing the reduction in droplet species, and increasing the ion production. Further investigation is necessary to verify this hypothesis.

The magnetic field affected the small mass species observed in the mass spectra. The ratio of the peak intensity of an ion measured during 200-Gauss magnetic field over the peak intensity of the same ion measured during zero magnetic field showed that the magnetic field created a mechanism which increased the energy of the ions. This was accentuated by higher concentrations of nanoparticles. The magnetic field effect was not statistically significant on the large mass distributions, however, it dropped the intensity of the 40,000 amu/e distribution observed in ILFF-30 spectra. This is motivation into future investigation of the magnetic effect on the larger masses of ILFF electrospray using a more repeatable method of measuring the mass distributions.

Acknowledgments

KJT would like to thank Marty Toth and Bill Langdon for machining all custom components for the experiments. All the authors would like to thank the Air Force Research Lab at Kirtland AFB for providing the facilities to conduct the testing. They would also like to thank the US Air Force Office of Scientific Research: International AOARD and Sirtex Medical Limited for funding the development of the ILFFs, and Steve Jones and Stephanie Bickley for designing and preparing the monodomain magnetic particles. The material is based upon work supported by NASA under award No NNX13AM73H. Any opinions, findings, and conclusions or recommendations expressed in this material are those of the authors and do not necessarily reflect the views of the National Aeronautics and Space Administration. BDP acknowledges support from the Air Force Office of Scientific Research under task number 16RVCOR275 (Program Manager: Michael Berman).

References

1. Rosensweig, R.E., "Magnetic Fluids," Annual Review of Fluid Mechanics, 19, 1987, pp. 437-461
2. Boudouvis, A.G., J.L. Puchalla, L.E. Scriven, and R.E. Rosensweig, "Normal field instability and patterns in pools of ferrofluid," Journal of Magnetism and Magnetic Materials, 65, 1987, pp. 307-310
3. Baker, G.A., S.N. Baker, S. Pandey, and F.V. Bright, "An analytical view of ionic liquids," Analyst, 130, 2005, pp. 800-808
4. Lozano, P.C., "Studies on the Ion-Droplet Mixed Regime in Colloid Thrusters," Department of Aeronautics and Astronautics, Massachusetts Institute of Technology, 2003
5. Legge, R.S., Jr., "Fabrication and Characterization of Porous Metal Emitters for Electrospray Applications," Department of Aeronautics and Astronautics, Massachusetts Institute of Technology, 2008
6. Gassend, B.L.P., "A Fully Microfabricated Two-Dimensional Electrospray Array with Applications to Space Propulsion," Department of Electrical Engineering and Computer Science, Massachusetts Institute of Technology, 2007
7. Alexander, M.S., et al., "Electrospray Performance of Microfabricated Colloid Thruster Arrays," Journal of Propulsion and Power, 22, 2006, pp. 620-627
8. Courtney, D.G., "Ionic Liquid Ion Source Emitter Arrays Fabricated on Bulk Porous Substrated for Spacecraft Propulsion," Department of Aeronautics and Astronautics, Massachusetts Institute of Technology, 2011
9. Coffman, C.S., "Considerations for a multi-modal electrospray propulsion system," Department of Aeronautics and Astronautics., Massachusetts Institute of Technology, 2012
10. Meyer, E.J., Lyon B. King, "Electrospray from an Ionic Liquid Ferrofluid utilizing the Rosensweig Instability " *49th AIAA/ASME/SAE/ASEE Joint Propulsion Conference & Exhibit,* San Jose, CA, 14-17 July 2013
11. Meyer, E.J., Lyon B. King, Nirmesh Jain, and Brian S. Hawkett, " Ionic liquid ferrofluid electrospray with EMIM-NTf2 and ferrofluid mode studies with FerroTec EFH-1 in a non-uniform magnetic field " *33rd International Electric Propulsion Conference* The George Washington University, USA, 6 -10 October 2013
12. Jain, N., X. Zhang, B.S. Hawkett, and G.G. Warr, "Stable and Water-Tolerant Ionic Liquid Ferrofluids," ACS Applied Materials & Interfaces, 3, 2011, pp. 662-667
13. Terhune, K.J., Lyon B. King, Michael L. Hause, Benjamin D. Prince, Nirmesh Jain, Brian S. Hawkett, "Species measurements in the beam of an ionic liquid ferrofluid electrospray source," *50th AIAA/ASME/SAE/ASEE Joint Propulsion Conference & Exhibit,* Cleveland, OH, 28-30 July 2014
14. Chiu, Y.H., et al., "Vacuum electrospray ionization study of the ionic liquid, [Emim][Im]," International Journal of Mass Spectrometry, 265, 2007, pp. 146-158
15. Jackson, G.P. and D.C. Duckworth, "Electrospray mass spectrometry of undiluted ionic liquids," Chemical Communications, 0, 2004, pp. 522-523
16. Dyson, P.J., et al., "Direct probe electrospray (and nanospray) ionization mass spectrometry of neat ionic liquids," Chemical Communications, 0, 2004, pp. 2204-2205
17. Fernández de la Mora, J., et al., "Electrochemical processes in electrospray ionization mass spectrometry," Journal of Mass Spectrometry, 35, 2000, pp. 939-952
18. Jain, N., et al., "Optimized steric stabilization of aqueous ferrofluids and magnetic nanoparticles," Langmuir, 2009, pp.
19. Rosensweig, R.E., *Ferrohydrodynamics* 1985, Mineola: Dover Publications, Inc.
20. King, L.B., et al., "Self-Assembling Array of Magnetoelectrostatic Jets from the Surface of a Superparamagnetic Ionic Liquid," Langmuir, 30, 2014, pp. 14143-14150
21. Madden, A., J. Fernández de la Mora, B. Hawkett, and N. Jain, "Effect of a homogeneous magnetic field on the electrospraying characteristics of sulfolane ferrofluids," *Unpublished Manuscript*, Yale University, 2016
22. Jackson, B.A., "Characterization of an Ionic Liquid Ferrofluid Electrospray Emission Pattern," *50th AIAA/ASME/SAE/ASEE Joint Propulsion Conference & Exhibit,* Cleveland, OH, 28-30 July 2014
23. den Hartog, S., "Ionic liquid ferrofluid electrospray: A new satellite propulsion system," Michigan Technological University, 2015
24. Terhune, K.J., et al., "The effects of magnetic surface stress on electrospray of an ionic liquid ferrofluid," *52nd AIAA/SAE/ASEE Joint Propulsion Conference,* Salt Lake City, UT, 25-27 July 2016
25. Gamero-Castaño, M., "Characterization of the electrosprays of 1-ethyl-3-methylimidazolium bis(trifluoromethylsulfonyl) imide in vacuum," Physics of Fluids, 20, 2008, pp. 032103

26. Krpoun, R. and H.R. Shea, "Integrated out-of-plane nanoelectrospray thruster arrays for spacecraft propulsion," Journal of Micromechanics and Microengineering, 19, 2009, pp. 045019
27. Chiu, Y.-H., et al., "Mass Spectrometric Analysis of Colloid Thruster Ion Emission from Selected Propellants," Journal of Propulsion and Power, 21, 2005, pp. 416-423
28. Romero-Sanz, I., R. Bocanegra, J.F. de la Mora, and M. Gamero-Castano, "Source of heavy molecular ions based on Taylor cones of ionic liquids operating in the pure ion evaporation regime," Journal of Applied Physics, 94, 2003, pp. 3599-3605
29. Chiu, Y.-H., et al., "Mass Spectrometric Analysis of Ion Emission for Selected Colloid Thruster Fuels," *39th AIAA/ASME/SAE/ASEE Joint Propulsion Conference and Exhibit*, Huntsville, Alabama,
30. Miller, S.W., B.D. Prince, R.J. Bemish, and J.L. Rovey, "Mass Spectrometry of Selected Ionic Liquids in Capillary Electrospray at Nanoliter Volumetric Flow Rates," *52nd AIAA/SAE/ASEE Joint Propulsion Conference*, Salt Lake City, UT,
31. Fernández de la Mora, J. and I.G. Loscertales, "The current emitted by highly conducting Taylor cones," Journal of Fluid Mechanics, 260, 1994, pp. 155-184
32. Fernández de la Mora, J., "The Fluid Dynamics of Taylor Cones," Annual Review of Fluid Mechanics, 39, 2006, pp. 217-243
33. Higuera, F.J., "Flow rate and electric current emitted by a Taylor cone," Journal of Fluid Mechanics, 484, 2003, pp. 303-327
34. Gañán-Calvo, A.M., "On the theory of electrohydrodynamically driven capillary jets," Journal of Fluid Mechanics, 335, 1997, pp. 165-188
35. Gamero-Castaño, M. and J. Fernández de la Mora, "Direct measurement of ion evaporation kinetics from electrified liquid surfaces," The Journal of Chemical Physics, 113, 2000, pp. 815-832
36. Garoz, D., et al., "Taylor cones of ionic liquids from capillary tubes as sources of pure ions: The role of surface tension and electrical conductivity," Journal of Applied Physics, 102, 2007, pp. 064913-10
37. Gamero-Castaño, M., "Electric-Field-Induced Ion Evaporation from Dielectric Liquid," Physical review letters, 89, 2002, pp. 147602